buildings

MDPI

Article

Retrofitting Towards Net-Zero Energy Building Under Climate Change: An Approach Integrating Machine Learning and Multi-Objective Optimization †

Mahdi Ibrahim [1,2,*], Pascal Biwole [2,3,4], Fatima Harkouss [5], Farouk Fardoun [5] and Salah Eddine Ouldboukhitine [1]

[1] CNRS, SIGMA Clermont, Institut Pascal, Université Clermont Auvergne, 63000 Clermont–Ferrand, France
[2] CNRS, LMPS—Laboratoire de Mécanique Paris-Saclay, ENS Paris-Saclay, CentraleSupélec, Université Paris-Saclay, 91190 Gif-sur-Yvette, France
[3] MINES Paris, PSL Research University, PERSEE—Center for Processes, Renewable Energies and Energy Systems CS 10207, Sophia Antipolis, 06904 Antibes, France
[4] School of Engineering, California State Polytechnic University, Arcata, CA 95521, USA
[5] Faculty of Engineering, Al Maaref University, Beirut 1600, Lebanon
* Correspondence: mahdi.ibrahim@ens-paris-saclay.fr
† This paper is an extended version of our paper published in Ibrahim, M.; Harkouss, F.; Biwole, P.; Fardoun, F.; Oultboukhtine, S. Building retrofitting towards net zero energy under climate change. In Proceedings of the TMREES24Fr International Conference, Metz, France, 8–10 July 2024.

Abstract

Achieving Net-Zero Energy Building (NZEB) performance through retrofitting requires identifying optimal measures that effectively enhance energy efficiency. Determining these optimal retrofit strategies typically involves running thousands of building energy simulations, which imposes a substantial computational burden. To address this challenge, a novel machine learning-based framework is proposed to optimize retrofit strategies for NZEBs under future climate change scenarios. A Non-Dominated Sorting Genetic Algorithm (NSGA-III) is employed to minimize both annual energy consumption and the Predicted Percentage of Dissatisfied (PPD), while simultaneously ensuring net-zero energy balance, thereby generating a Pareto front of optimal solutions. The Technique for Order of Preference by Similarity to Ideal Solution (TOPSIS) is then applied to rank the Pareto-front solutions and identify the most favorable retrofit scenario. The results show that the proposed framework reduces optimization time by at least a factor of two compared with simulation-only optimization. Leveraging these computational savings, the framework evaluates a suite of passive and renewable measures across multiple future timeframes to capture the influence of climate change on retrofit performance. The findings indicate that achieving NZEB under future climate conditions requires higher levels of thermal insulation and greater renewable integration than under present-day conditions. Under the Shared Socioeconomic Pathways (SSP) framework, optimal insulation levels in the fossil fuel-dependent scenario are lower than in the sustainable scenario by up to 18% in C-type (warm temperate), 12% in D-type (snow), and 13% in E-type (polar) climates. The combined retrofit measures can reduce annual energy consumption by up to 80% and lower PPD by as much as 67% compared to the base case.

Keywords: Net-Zero Energy Building; building retrofitting; ANN surrogate model; NSGA-III; TOPSIS decision-making; climate change; machine learning

Check for updates

Academic Editor: Shi-Jie Cao

Received: 3 September 2025
Revised: 19 December 2025
Accepted: 26 December 2025
Published: 28 January 2026

Copyright: © 2026 by the authors. Licensee MDPI, Basel, Switzerland. This article is an open access article distributed under the terms and conditions of the Creative Commons Attribution (CC BY) license.

1. Introduction

High energy consumption remains a pressing global challenge driven by population growth and rising standards of living [1,2]. Net-zero energy buildings (NZEBs) have emerged as a sustainable response to mitigate the escalating energy demand and greenhouse gas emissions from the building sector, which is currently the third-largest energy consumer globally [3]. NZEBs are defined as low-energy buildings in which the annual energy demand is fully offset by on-site renewable energy production [4]. In alignment, the Energy Performance of Buildings Directive targets NZEB adoption across Europe by 2050, through the implementation of comprehensive renovation plans [5,6]. The urgent need for resilient retrofit pathways motivates research that accurately predicts building performance under present and future climatic conditions.

Building energy simulations (BESs) have extensively utilized Typical Meteorological Year (TMY) weather data due to their computational efficiency and ease of implementation in retrofit scenarios [7–12]. However, TMY data do not capture interannual variability or long-term climate trends. Several studies report substantial deviations between TMY-based estimates and multi-year or climate-projection-based outcomes, which can lead to biased retrofit decisions [12–15]. Multi-year and downscaled climate projections (e.g., CMIP5/6 scenarios) have therefore been adopted to quantify the sensitivity of retrofit performance to climate change, with recent works demonstrating notable implications for HVAC sizing, PV capacity, and long-term NZEB viability. Neto et al. [16] demonstrated that focusing only on HVAC retrofits is insufficient to maintain NZEB status under future climates. Luo et al. [17] introduced a life-cycle optimization framework considering climate change in tropical regions, reporting underestimations of energy use and emissions by up to 54.7% when relying on present-day weather. Shen et al. [18] projected energy demand changes across future climate scenarios, emphasizing the need to increase PV capacity by up to 20% to meet NZEB targets. Shen, Braham et al. [19] highlighted that excluding climate change considerations may bias retrofit outcomes by over 30%.

Multi-year weather datasets have been incorporated into multi-objective optimization (MOO) frameworks to quantify the impacts of climate change on building retrofit strategies. For example, Kim et al. [20] developed a MOO scheme for climate-adaptive envelope upgrades in hot, humid regions, targeting the minimization of cooling loads and the maximization of daylighting. Their results demonstrated that enhanced insulation and upgraded glazing, when evaluated over evolving weather profiles, substantially reduce energy use while maintaining comfortable daylight levels, thereby supporting both productivity and occupant well-being. Li et al. [21] extended this approach by formulating a robust retrofit optimization that simultaneously maximizes energy efficiency and minimizes life-cycle costs under diverse future climate scenarios. This study highlighted the critical role of accurate climate projections in guiding architects' decisions on cost-effective, energy-saving measures. Similarly, Zou et al. [22] applied a MOO framework to Guangzhou's climate, identifying representative future design years under various Representative Concentration Pathways; their findings indicate a projected mean temperature rise of 2.8 °C by 2100, reinforcing the need for long-term, climate-responsive retrofit planning.

Despite the advantages of MOO, its application to building retrofits is often constrained by the intensive computational demands of repeated building energy simulations (BES). Meta-modeling mitigates this bottleneck by training surrogate models on a limited set of BES outputs, thereby replicating full-scale simulations and permitting rapid performance evaluations across design variables. Common surrogate techniques include Multivariate Adaptive Regression Splines (MARS), polynomial regression, support vector machines (SVM), Gaussian processes (Kriging), and artificial neural networks (ANNs) [23–27]. In a comprehensive review, Starke et al. [24] reported that ANNs consistently outperform these

alternatives in high-dimensional optimization problems while scaling efficiently with large datasets. Zhan et al. [25] used an ANN meta-model to optimize building envelope, HVAC, and control upgrades. It was demonstrated that combinations of high-performance insulation and efficient HVAC systems provide the best compromise between annual energy use and life-cycle cost. Aruta et al. [26] embedded an ANN surrogate into a model predictive control scheme for space cooling, reporting 10–15% energy savings through optimized set-points and night-purge ventilation. Zhang et al. [27] implemented an ANN-driven decision-support tool to rank hundreds of retrofit packages. It was shown that top-ranked bundles systematically include improved insulation, high-efficiency heating systems, and advanced control strategies. To best of the authors' knowledge, these studies do not consider the joint effects of future climate scenarios on NZEB performance when using ANN surrogates. The present work addresses this gap by incorporating downscaled climate projections into an ANN-based MOO for NZEB retrofit design. First, it evaluates retrofit strategies across various cities representing different Köppen–Geiger climate zones, using projected weather data under climate change scenarios. Then, comprehensive optimization is performed considering parameters such as insulation levels, window U-values, infiltration rates, heating setpoints, and renewable system configurations. Finally, a multicriteria decision-making (MCDM) approach is employed to identify the most suitable solution for each scenario.

2. Materials and Methods

This section outlines the methodological framework employed to retrofit the reference case study building to achieve NZEB performance. The approach begins with the design of experiments aimed at generating a representative dataset, which serves as the foundation for training a machine learning model. Subsequently, the dataset is modified through mathematical transformations to reflect projected future climate scenarios. In the third stage, a multi-objective optimization problem is formulated using the ANN model to derive Pareto-front retrofit solutions. A MCDM technique is then applied to select the most suitable solution from the Pareto-front. The final two steps, optimization and decision-making, are iteratively conducted under varying climate scenarios and time horizons to assess the robustness of the retrofit strategies.

2.1. Reference Building

The base case study examines a residential building located in Cébazat, a village near Clermont-Ferrand, France. Constructed in 2010, the building comprises three stories and accommodates 17 apartments, as illustrated in Figure 1, with a total floor area of 1599.2 m^2.

The thermo-physical characteristics of the building envelope are presented in Table 1. The external walls incorporate a double-layer insulation system composed of Xtherm Itex 32E expanded polystyrene [28], providing a thermal resistance of R = 3.4 $W/m^2 \cdot °C$. The roof assembly includes cellulose fiber insulation (thermal conductivity of 0.125 $W/m \cdot °C$), overlaid with a wooden framework and Roman tiles. The fenestration consists of argon-filled double-glazed windows (4/16/4), characterized by a U-value of 1.4 $W/m^2 \cdot °C$ and a solar heat gain coefficient (G-value) of 0.6. These windows are mounted in PVC frames and lack external shading elements such as overhangs, blinds, or louvers.

The occupancy schedules for primary spaces, including the living room, bedroom, and kitchen, follow the guidelines specified in EN 18523-2 [29] and are illustrated in Figure 2. Each room is equipped with 60 W LED lighting. Standard household appliances installed in the apartments include a television (in the living room), as well as a refrigerator, microwave, washing machine, dishwasher, and iron (in the kitchen). Kitchen ventilation is provided by single-flow, humidity-sensitive mechanical exhaust fans.

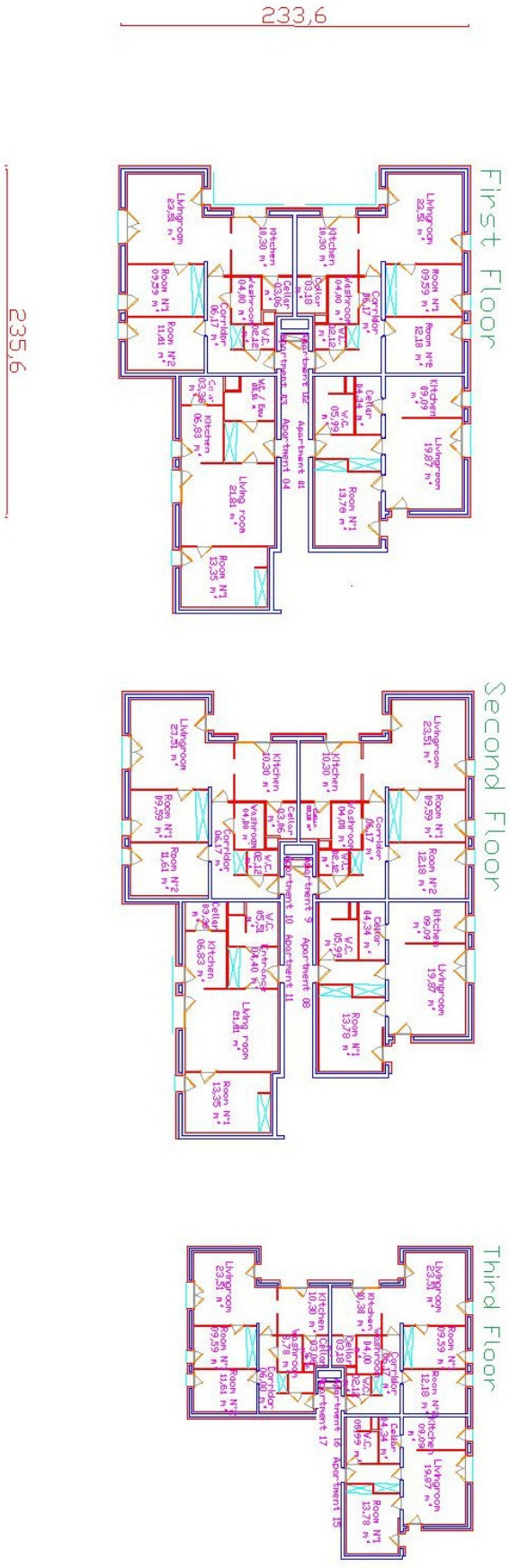


Figure 1. Plan view of the base-case building (dimensions in 10 cm).

Table 1. Thermo-physical properties of the base case building's envelope.

Components	U-Value Coefficient (W/m^2.°C)	Layers (Out to in)	Thickness (cm)	Thermal Conductivity (W/m.°C)
External Wall	0.12	Wood cladding	1	0.2
		Expanded polystyrene	15	0.0309
		Concrete	18	0.46
		Expanded polystyrene	10	0.0309
		Plaster (BA13)	13	0.32074
Internal Wall	0.25	Concrete	18	0.46
		Expanded polystyrene	15	0.0309
Ground Floor Wall	0.3	Concrete deck	23	0.46
		Extruded polystyrene	15	0.029
Roof	0.16	Insulation material (U = 0.125 W/m^2.°C)	20	0.0625
		Timber concrete	13	1.3

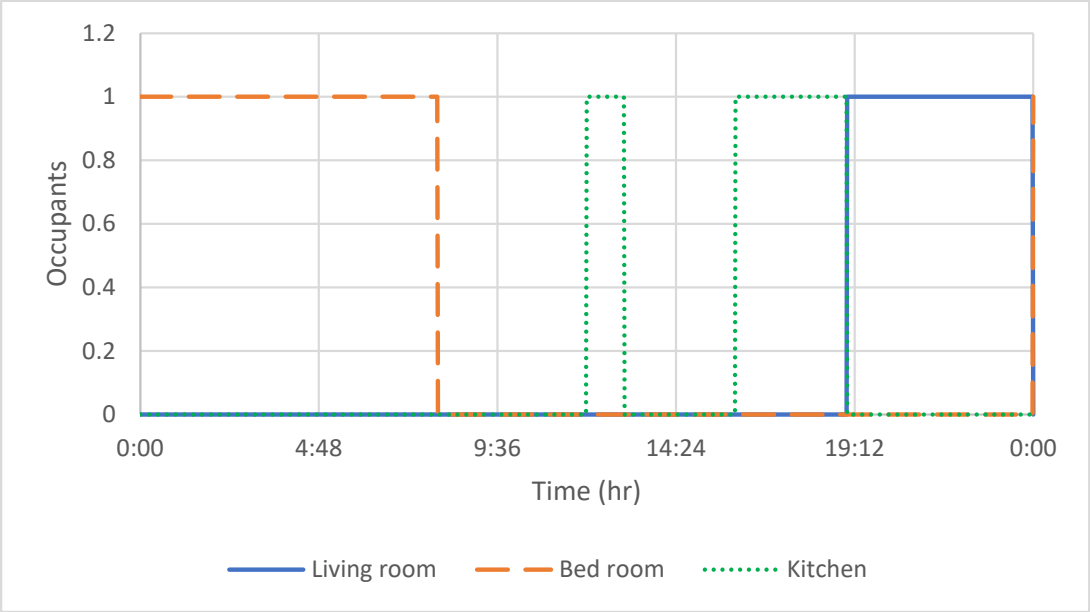


Figure 2. Daily Schedule of occupancy for different rooms.

Space heating is delivered through individual condensing gas boilers, one per apartment, each connected to a radiator network. These boilers have a storage capacity of 42 L and a nominal thermal output of 23 kW. In accordance with EN 625 [30], the domestic hot water (DHW) system delivers water at a flow rate of 18.5 L/min, with supply and return temperatures of 45 °C and 40 °C, respectively. The DHW consumption profile, based on hourly data provided by the French Agency for the Environment and Energy Management [31], is shown in Figure 3. Annual DHW demand is computed by scaling this profile with monthly adjustment factors.

2.2. Design of Experiments

The reference building model was developed in TRNSYS (Transient System Simulation Tool), a widely used BES platform. To ensure the reliability of the simulation results, a calibration procedure was performed to validate the TRNSYS outputs [32–35]. Both passive

and renewable retrofit measures were incorporated into the TRNSYS model and served as inputs for training the ANN. Key ANN input variables include climatic parameters, dry-bulb temperature, direct and diffuse solar radiation, relative humidity, wind speed, and wind direction, as well as a time-step index ranging from 1 (first hour of January 1) to 8760 (final hour of December 31) to capture hourly variations over the year [36,37].

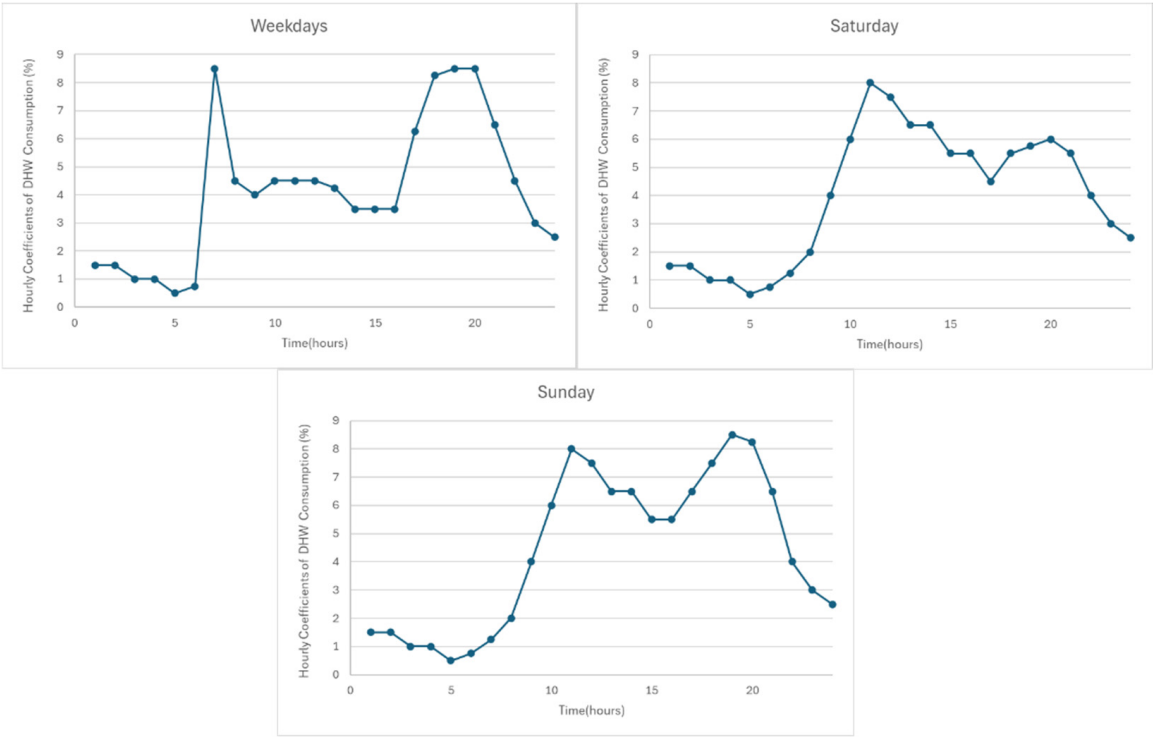


Figure 3. Hourly profile of DHW consumption over a week.

Passive envelope upgrades target the building's thermal barrier, comprising exterior walls, windows, and air leakage controls. Based on an extensive literature review [4,5,31,33,38–46], the retrofit measures most applicable to the case study include window glazing U-value, infiltration rate, external wall insulation thickness, and the thickness of radiant ceiling panels, all using expanded polystyrene consistent with the original construction. These enhancements aim to reduce heat losses and meet the building's heating load more efficiently.

Renewable systems were selected to satisfy the building's residual energy demands. A solar domestic hot water (SDHW) system, equipped with an auxiliary electric heater within the storage tank, was roof-mounted to provide all domestic hot water needs. Electrical loads are met by a rooftop photovoltaic (PV) array in conjunction with a small-scale domestic wind turbine.

(a) Solar domestic hot water system characteristics

The SDHW system employs a series of solar collectors totaling 31.35 m^2 of aperture area [44]. The number of collectors is treated as an optimization variable and is therefore included among the inputs to the ANN. All collectors face due south and are tilted at 45.78°, corresponding to the site's latitude. The key system specifications are summarized in Table 2.

Table 2. Technical characteristics of the SDHW system [47].

Characteristics	Value	Unit	Note/Comment
Collector area	2.09	m^2	Rounded from original value
Collector flow rate	60	kg/h	Expressed as mass flow rate
Storage volume	2.271	m^3	Total hot-water storage volume
Hot water set point	60	°C	Controller set point
Hot water supply temperature	45	°C	Expected supply temperature
Intercept efficiency	0.79	kg/h	Can be reported as 79%
Efficiency slope	3.48	$W/m^2.K$	Rounded (original: 3.48)
Efficiency curvature	0.0056	$W/m^2.K^2$	Rounded (original: 0.0056)

A control dead band of 5 °C temperature differential between the tank inlet and outlet triggers the circulation pump when reached; the pump deactivates once this differential falls below 2 °C. To safeguard against thermal runaway, a high-temperature cutoff at 90 °C is monitored at the apex of the tank. If the tank reaches this temperature, the pump is automatically disabled to prevent boiling within the storage vessel.

(b) PV system characteristics

A photovoltaic (PV) array of monocrystalline silicon modules is deployed to meet the building's electrical demand. The array is inclined to the south at an angle equal to the site's latitude and its geometric area (m^2) is computed via Equation (1) [48]. Module specifications appear in Table 3. A temperature correction factor (TCF) of 0.80 is applied to account for a 15–20% reduction in conversion efficiency at elevated cell temperatures approaching 60 °C [49]. The DC-AC inverter operates at 97% efficiency [50]. The array's peak power output is calculated using Equation (2), with the series–parallel configuration of the modules adjustable to achieve the required DC bus voltage and current [51].

$$PV_{area} = \frac{E_L}{G_{av} \times \eta_{PV} \times TCF \times \eta_{Jnv}} \quad (1)$$

$$PV_{Peak\ power} = PV_{area} \times PSI \times \eta_{PV} \quad (2)$$

where

- E_L represents the daily electrical load (kWh/day).
- G_{av} denotes the average irradiation available per day (kWh/m^2·day).
- η_{PV} stands for the PV efficiency.
- TCF is the temperature correction factor.
- η_{Jnv} represents the inverter efficiency.
- PSI indicates the Peak Solar Irradiance (W/m^2).

Results from these calculations are summarized in Table 3. Surplus PV generation is exported to the utility grid, while deficits are met by grid imports. This grid-tied configuration obviates the need for battery storage, thereby minimizing energy losses, system complexity, and maintenance requirements associated with on-site energy storage [46,52].

(c) Domestic wind turbine

The results from these calculations are summarized in Table 3. Surplus PV generation is exported to the utility grid, while deficits are met by grid imports. This grid-tied configuration obviates the need for battery storage, thereby minimizing energy losses, system complexity, and maintenance requirements associated with on-site energy storage [46]. Technical specifications for the wind turbines are provided in Table 4. The required turbine quantity to meet the target power output will be determined during the optimization phase. In TRNSYS, the turbines are represented using the Type 90 model.

Table 3. Technical characteristics of PV [53].

Characteristics	Value	Characteristics	Value
Short circuit current (A)	9.32	Temperature coefficient of open circuit voltage (V/K)	−0.318
Open circuit voltage (V)	45.92	Module efficiency	% 17
Current at maximum power (A)	8.85	Temperature coefficient of short circuit current (A/K)	0.042
Panel area (m^2)	1.94	Nominal output (Wp)	295.3

Table 4. Technical characteristics of the domestic wind turbine [54].

Specification	Value
Nominal (rated) electrical power	1.3 kW
Cut-in (start-up) wind speed	3 m/s
Nominal wind speed for rating	11 m/s
Rotor diameter	2.9 m
Hub (tower) height to nacelle	14.5 m
Rotor configuration	3 blades, horizontal axis
Rotational speed at nominal power	800 rpm

Following the definition of weather parameters, as well as passive and renewable retrofit measures, training data were generated using BES. These simulations provided the foundation for constructing the ANN surrogate model. To ensure representative and efficient sampling of the input parameter space, Latin Hypercube Sampling (LHS) is employed, in accordance with the approach reviewed by Westermann et al. [23]. LHS adopts a stratified sampling strategy in which the range of each input variable is divided into equally probable intervals. From each interval, a single sample is randomly selected, ensuring that the entire domain of each parameter is represented without redundancy. This method improves the uniformity of the sampling distribution across the multidimensional input space and avoids clustering or oversampling in specific regions [55]. As a result, the LHS approach generates a well-distributed and comprehensive training dataset that captures the full variability of the defined weather, passive, and renewable retrofit parameters. This diversity in the training data enhances the accuracy, robustness, and generalizability of the ANN surrogate model. In line with the recommendation of Jones, Schonlau, and Welch [50], which recommends that simulation datasets for surrogate models be at least ten times the number of inputs, 200 annual BES runs were generated. These 200 annual simulations produced approximately 1.752 million hourly records (200 × 8760 h), forming the dataset used to train and validate the surrogate models.

2.3. Artificial Neural Network Model Development

The data generated from the previous steps are employed to train the ANN model. The architecture of the ANN is determined through the Multi-Objective Hyperparameter Optimization of ANN (MOHO-ANN) method, as proposed by Ibrahim et al. [56,57]. This methodology results in a five-layer ANN architecture comprising 321 neurons, with the Gaussian Error Linear Unit (GELU) used as the activation function. The model is trained using the Adam optimizer with a learning rate of 0.00001, a batch size of 70, and zero dropout. The ANN is developed to predict three key performance indicators on an hourly basis: energy consumption, energy generation, and thermal comfort, represented by the Predicted Mean Vote (PMV). These predictions are based on hourly weather data inputs, along with parameters that define passive and renewable retrofit measures. Figure 4 illustrates the comparison between the ANN-predicted outputs and the TRNSYS-simulated results for the baseline case study. The ANN demonstrates high predictive performance, achieving coefficients of determination (R^2) of 0.987 for energy demand, 0.994 for energy

generation, and 0.999 for PMV. These results indicate a strong agreement between the ANN predictions and the detailed TRNSYS simulations, confirming the accuracy and reliability of the surrogate model.

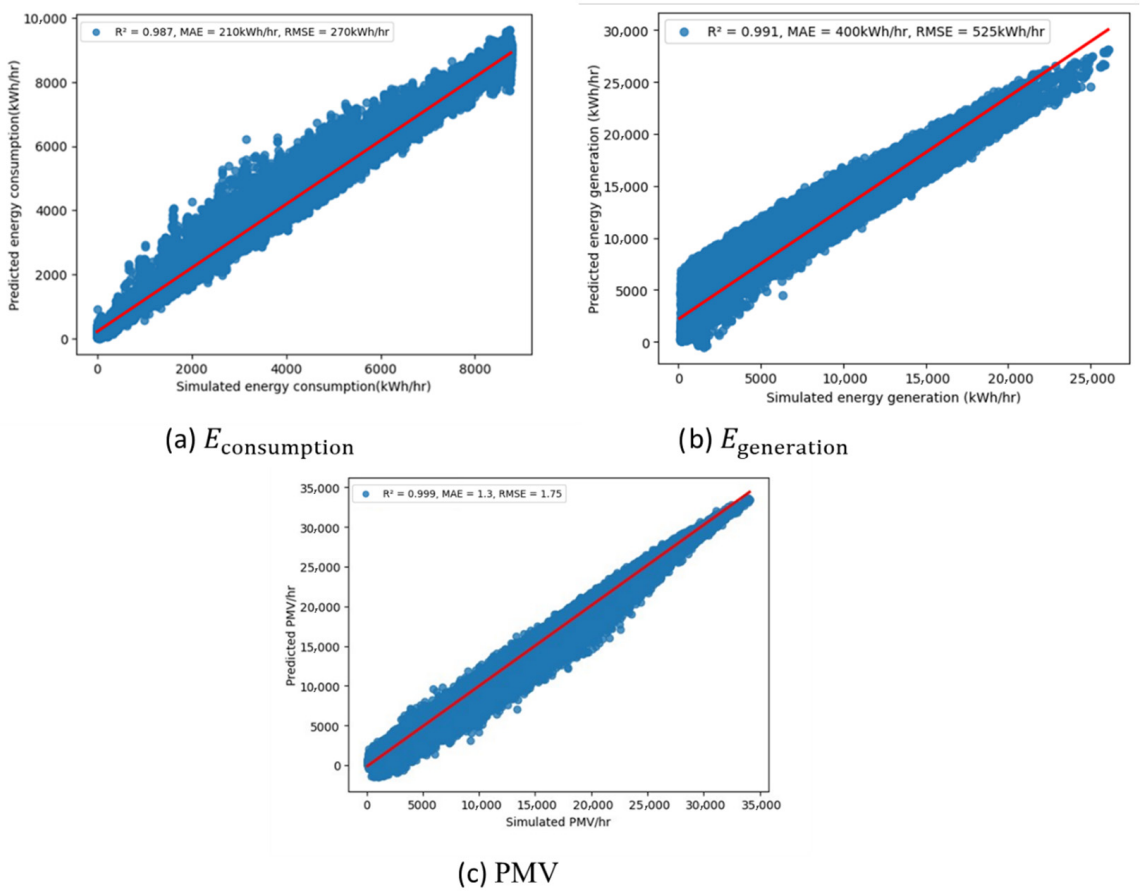


Figure 4. Regression plot of ANN model outputs.

A 5-fold cross-validation protocol was applied to obtain stable performance estimates and mitigate ANN overfitting, following the procedure recommended by Abbass et al. [51]. The dataset was partitioned into five equal folds; in each iteration, the model was trained on four folds and validated on the remaining fold, so that every observation contributed to both training and validation. Model performance was quantified using the R^2 computed on the validation sets. Figure 5 presents a box plot of the cross-validation R^2 distribution. The median R^2 is 0.88, the interquartile range (IQR) spans 0.86–0.90, and the whiskers extend from 0.84 to 0.92, indicating high predictive accuracy and low variability across folds. The narrow IQR and limited whisker length imply stable model behavior with no substantial outliers, supporting the ANN's capacity to generalize to unseen data and thereby reducing the risk of overfitting. In the plot, the light-blue boxes denote the IQR and the red lines the medians; the compact spread further evidences the model's reliability across heterogeneous data subsets, which is essential for real-world applications.

2.4. Optimization Problem Formulation

In this study, the optimization process is performed using the ANN model implemented within the PyTorch framework [58], in conjunction with the Pymoo library, an advanced Python 3.10-based platform for MOO developed by Blank et al. [53]. Pymoo has been recognized for its superior computational performance in building energy modeling applications, outperforming alternative MOO tools such as MOBO and Dakota, as reported

by El Kounni et al. [54]. The complete workflow of the building optimization process, including its sequential phases, is illustrated in Figure 6.

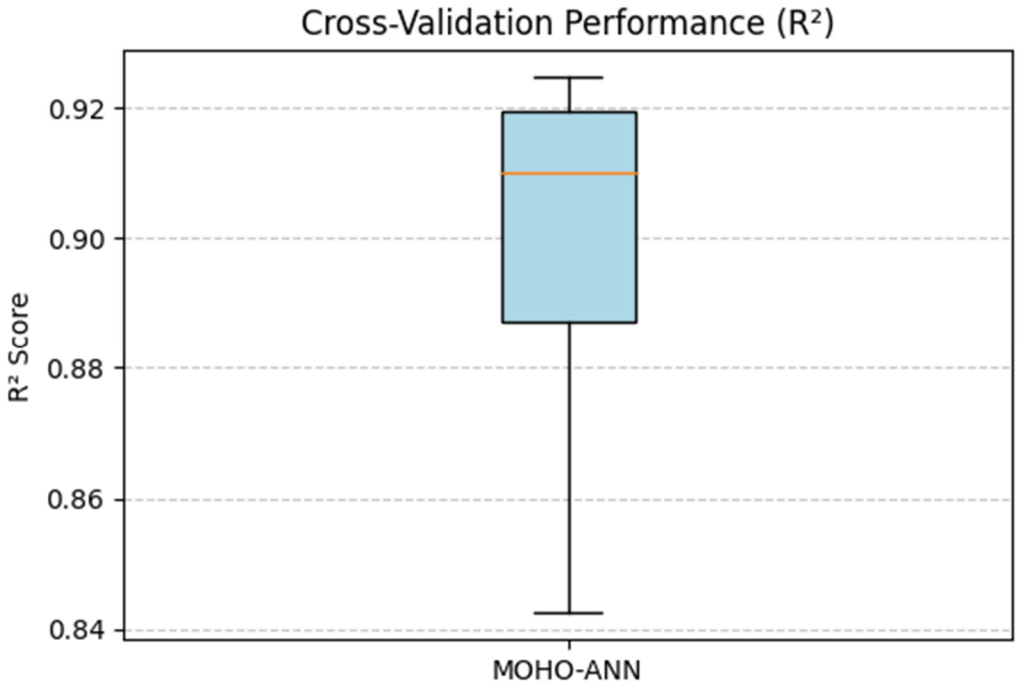


Figure 5. Five-fold cross-validation R^2 scores for the ANN.

The multi-objective optimization framework employed is used to minimize both the building's energy consumption and its annual average Predicted Percentage of Dissatisfied (PPD). Accordingly, the optimization problem can be summarized as follows:

$$\begin{cases} Min(\mathrm{E_{consumption}}) \\ Min(\mathrm{PPD}) \end{cases} \quad (3)$$

Annual energy balance constitutes a fundamental element in defining NZEB within the optimization framework. The building's total annual energy consumption must be counterbalanced by energy produced through renewable retrofit measures to satisfy this criterion. Consequently, constraints are imposed on both annual energy consumption and generation within the optimization problem. In accordance with ASHRAE Standard 228 [55], a permissible difference of 1 kWh·m^{-2}·year^{-1} between consumption and generation is typically adopted. This relationship is expressed by the following equation [59–63]:

$$\sum(\mathrm{E_{consumption}} \times SF_{consumption}) - \sum(\mathrm{E_{generation}} \times SF_{generation}) = E_{net} \quad (4)$$

where

- $\mathrm{E_{consumption}}$: total annual energy consumption (kWh/year)
- $SF_{consumption}$: source energy factor for consumed energy [62]
- $\mathrm{E_{generation}}$: total annual energy generation (kWh/year)
- $SF_{generation}$: source energy factor for generated energy [62]
- E_{net}: net source energy which represents the difference value (1 kWh/year in the case studied)

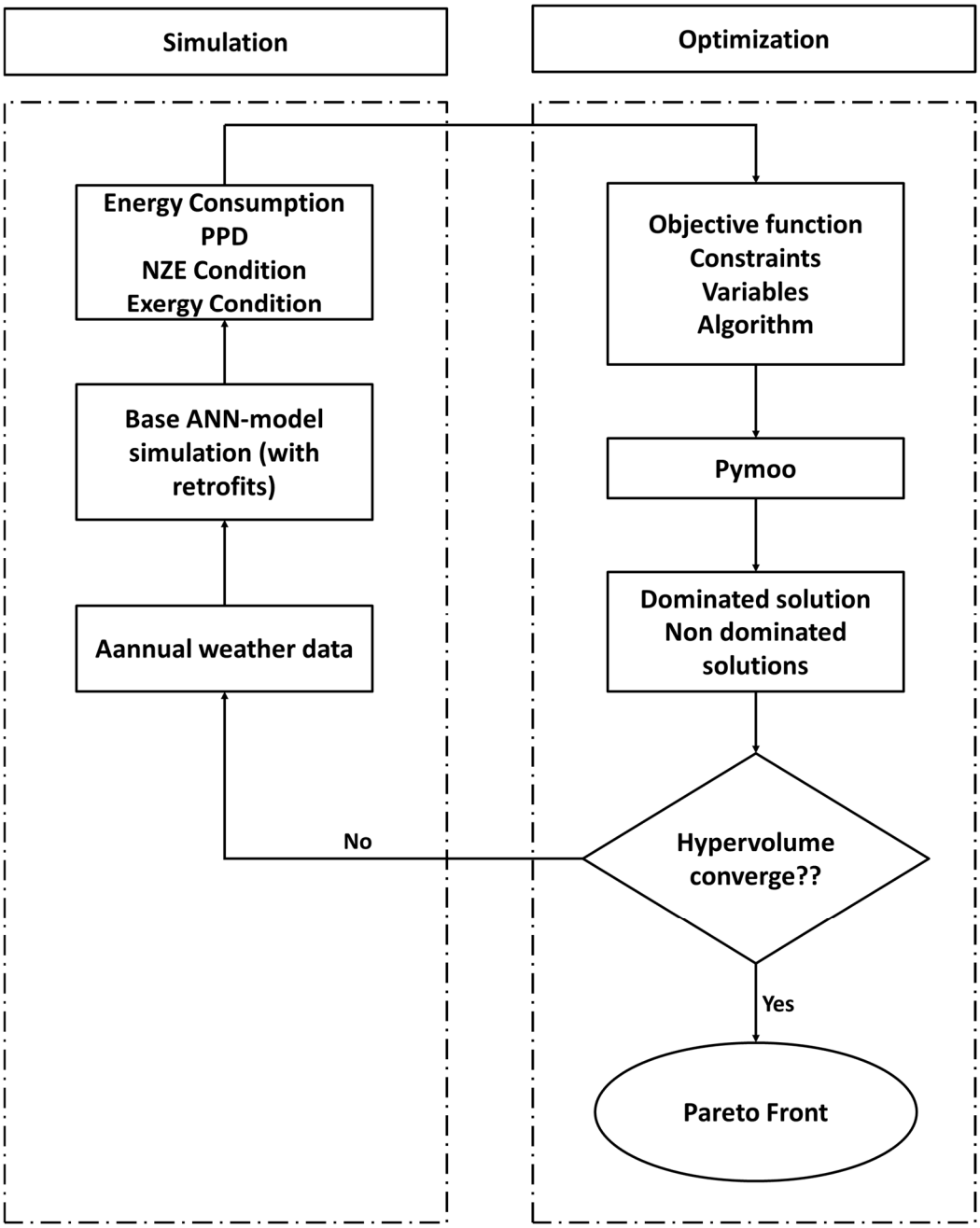


Figure 6. Optimization phase of the ANN model.

Table 5 presents the different sets of retrofit measure decision variables employed during the optimization of the ANN model parameters, excluding time-step and weather inputs to enforce the aforementioned constraints. For each decision variable, the table specifies the allowable range of values used during the optimization process. An optimal combination of these variables will be determined for each solution set and region to achieve NZE balance while minimizing the previously defined objective functions. This scenario-based approach facilitates a systematic comparison of retrofit strategies and their relative effectiveness in achieving net-zero energy targets across different building types and climatic conditions.

Table 5. Different employed sets of retrofit-measure decision variables.

Retrofit Measure Type	Retrofit Measure	Interval	Unit	Type
Passive retrofit measures	External wall insulation thickness	1–40	cm	Integer
	Window U-value	0.5–6.4	$W/m^2.K$	Float
	Roof wall insulation thickness	1–40	cm	Integer
	Heating setpoint temperature	15–23	°C	Integer
	Infiltration rate	0–0.6	Air change per hour (ACH)	Float
Renewable retrofit measures	Number of PV in series	1–40	-	Integer
	Number of PV in parallel	1–40	-	Integer
	Number of SC	1–40	-	Integer
	Number of WT	1–4	-	Integer

The non-dominated sorting genetic algorithm-III (NSGA-III), introduced by Deb et al. [64], was employed for this optimization. It extends NSGA II's strengths, including elitism, feasibility handling, and non-dominated sorting. NSGA III improves accuracy in many objective problems and those with complex constraints [6,31]. Although NSGA-II consistently generates well-distributed Pareto fronts and strong trade-off solutions for bi-objective building-performance problems [65], NSGA-III has demonstrated superior performance in capturing higher-dimensional Pareto sets and delivering more precise optimal fronts.

The NSGA-III workflow is defined by population size and stopping criteria, followed by crossover and mutation operations. The input parameters adopted in this study are listed in Table 6. These settings were selected based on preliminary analyses to balance Pareto-front accuracy with computational efficiency [34,66].

Table 6. NSGA-III optimization parameters.

Parameter	Values
Population size	40
Stopping criteria	Hypervolume convergence
Crossover probability %	70
Mutation probability %	2

2.5. Multi-Criteria Decision Making

Selecting an optimal solution from the Pareto-front requires integrating decision-maker preferences from regulators, tenants, landlords, architects, and engineers using the TOPSIS outranking method [67,68]. TOPSIS ranks non-dominated solutions by their Euclidean distance to ideal and anti-ideal points and is widely used in MCDM [63,65,67–76]. Objective-function weights are then determined via Saaty's Analytic Hierarchy Process (AHP) to reflect the relative importance of each criterion [71,72].

Variations in objective function weights can significantly impact the final outcome. Therefore, a sensitivity analysis is needed to examine their impact on the optimal solution. Seven cases are defined to assess the robustness of ranking from the decision-maker'ss perspective. Table 7 presents the relative weights for each case, representing different levels of importance. Case 1 assumes equal importance. Cases 2 and 3 assign moderate importance to one function over the other. Cases 4 and 5 assign strong importance. Cases 6 and 7 assign extreme importance.

Figure 7 summarizes the methodology for the sensitivity analysis. The ranking of optimal points remains consistent across all decision-maker preference sets, climate zones, and time frames. This consistency indicates that the selected retrofit measure is robust and not highly sensitive to variations in objective-function weights.

Table 7. Relative weights for each objective function across several cases.

Cases	Weights	
	F_1	F_2
Case 1	0.5	0.5
Case 2	0.6	0.4
Case 3	0.4	0.6
Case 4	0.75	0.25
Case 5	0.25	0.75
Case 6	0.9	0.1
Case 7	0.1	0.9

F_1 : $E_{consumption}$, F_2 : PPD.

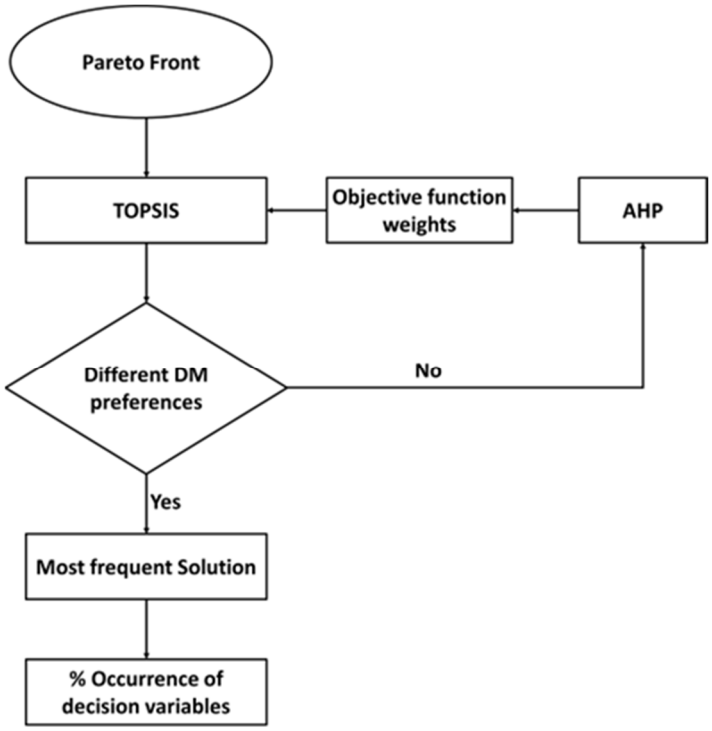


Figure 7. Sensitivity analysis methodology.

2.6. Future Weather Files Generation and Climate Extension

Future weather files are required for the ANN model to identify optimal NZEB retrofit measures under climate change. Present-day weather data are morphed to match projections from a numerical climate model. This procedure transforms historical meteorological records so that they are statistically consistent with future climate scenarios.

Two Shared Socioeconomic Pathways (SSPs) are selected to represent contrasting futures. SSP1-2.6 describes a sustainable development trajectory with aggressive mitigation. Under this scenario, CO_2 emissions fall to net zero by the mid-century, and global temperature rises are limited to about 1.7 °C by 2100 [73,74]. It combines the low-forcing RCP2.6 pathway, which peaks near 3 W/m^2 before declining to 2.6 W/m^2, and sustainability-focused socioeconomic assumptions. In contrast, SSP5-8.5 envisions continued reliance on fossil fuels and high emissions. Radiative forcing under RCP8.5 reaches roughly 8.5 W/m^2 by 2100, driving temperature increases of about 4.3 °C [75]. This scenario pairs rapid economic growth with minimal mitigation efforts and a heavy dependence on non-renewable energy. Building-level sustainability assessment should be included when evaluating retrofit and resilience strategies under these SSPs. Such assessment must address both em-

bodied and operational impacts, since structural typology and design choices can strongly influence seismic resilience and environmental outcomes [76].

To cover diverse climates, the Köppen–Geiger classification [77] is adopted. It divides regions into five main zones, including equatorial (A), arid (B), warm-temperate (C), snow (D), and polar (E), based on precipitation and temperature thresholds. Subclasses denote precipitation patterns (W, S, f, s, w, m) and temperature regimes (h, k, a, b, c, d, F). Since the ANN focuses on heating loads, tropical (A) and arid (B) climates were excluded from the analysis. Table 8 lists the three selected cities, including their respective latitudes, longitudes, and altitudes.

Table 8. Climate characteristics of the selected cities based on the Köppen–Geiger classification [69].

City	Climate	Altitude (m)	Latitude	Longitude
Cébazat (France)	Oceanic climate (Csb)	321	45.46 N	3.04 E
Chita (Russia)	Monsoon-influenced subarctic climate (Dwc)	671	113.33 E	52.02 N
Resolute (Canada)	Polar climate (ET)	2550	81.54 N	75.654 W

3. Results and Discussion

3.1. Optimization Phase

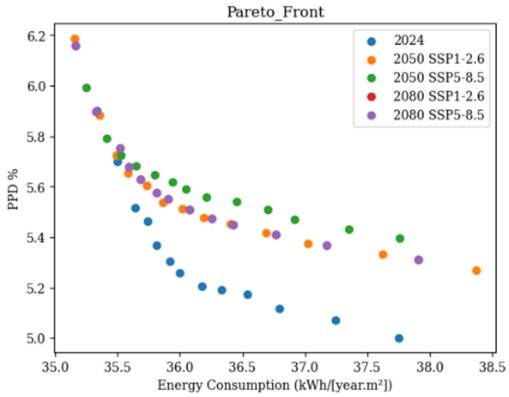
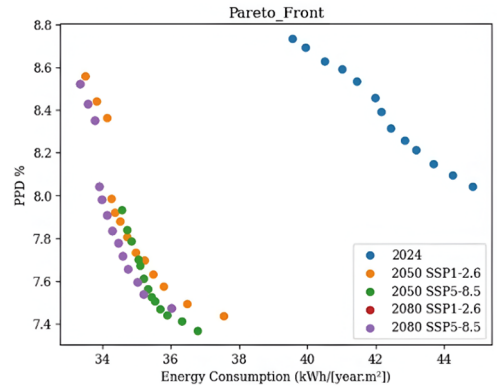
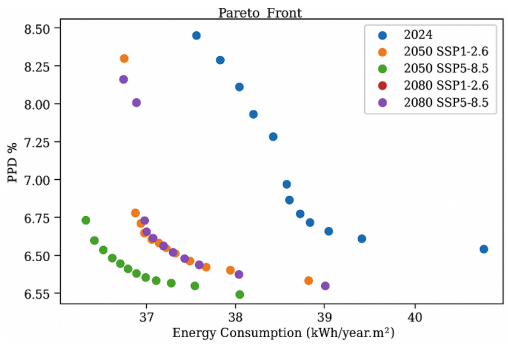
In multi-objective optimization, a single solution that simultaneously optimizes all objectives cannot be obtained. Instead, attention is focused on Pareto-front solutions, which are not dominated by any other solution and cannot be improved in one objective without degrading at least one other objective.

Table 9 lists the Pareto-front solutions for NZEB under different time horizons and climate zones. Each Pareto-front plot displays annual specific energy consumption (kWh/[year.m^2]) on the horizontal axis and PPD % on the vertical axis. Five scenarios are shown: present day (2024, blue), mid-century under SSP1-2.6 (2050, orange), mid-century under SSP5-8.5 (2050, green), late-century under SSP1-2.6 (2080, red), and late-century under SSP5-8.5 (2080, purple). Within each climate zone, the Pareto-fronts are nearly parallel, exhibiting only minor shifts. An inverse relationship is apparent between energy consumption and PPD, as lowering occupant discomfort in winter necessitates higher heating loads and, consequently, greater energy use.

Hypervolume measures the volume between a reference point and all Pareto-front solutions. Stabilization of this hypervolume with increasing iterations indicates algorithmic convergence. Table 9 reports the iteration count at which hypervolume stabilization occurs for each climate zone. Cébazat city (classified as C) requires between 1030 and 1592 iterations, whereas zones such as Resolute and Chita require between 1550 and 2088 iterations. This difference arises because the ANN model was trained on a low-energy building in a C-type climate, making NZE balance more rapidly attainable under similar conditions. These findings highlight the need for climate-specific model calibration and raise questions about the model's generalizability to non-C climates, where additional adaptation may be necessary.

The MOHO-ANN workflow described by Ibrahim et al. [56,57] delivers significant computational speedups relative to traditional methods. For the case study building, dataset generation, hyperparameter tuning, and ANN training required six simulation days. Retrofit optimization on this ANN then took 166 min for 1000 genetic-algorithm iterations [4]. By contrast, a conventional physics-based building energy simulation, coupled with the same genetic algorithm, would take more than 11 days. Thus, the ANN-based approach achieves at least a twofold reduction in optimization time.

Table 9. Pareto-front representation of different climate zones and time frame scenarios.

Climate Type	Climate Zone	Pareto-Front	Hypervolume Convergence Point				
			Normal	2050 SSP1-2.6	2050 SSP5-8.5	2080 SSP1-2.6	2080 SSP5-8.5
Warm Temperate Climate (C)	Cébazat (Csb)		1030	1260	1250	1588	1592
Polar Climate (E)	Resolute (ET)		2100	2166	2155	2255	2030
Snow Climate (D)	Chita (Dwc)		1550	1874	1920	2050	2088

3.2. Multi-Criteria Decision-Making Phase

Table 10 summarizes the retrofit measures derived from the decision-making phases for all examined climate zones and time frames, spanning a broad range of future conditions. These results indicate significant potential for achieving NZEB through passive envelope upgrades across diverse climates.

Insulation thickness in the building envelope depends on both climate zone and time frame. Optimal retrofit strategies for exterior walls and roofs require substantially greater insulation levels. A 1 cm layer of insulation on walls or roofs is therefore insufficient to safeguard the building envelope under any of the examined climatic conditions or time horizons. In the C-type climate represented by Cébazat, where heating demand is relatively low, insulation thickness ranges from 3 cm in the 2080 SSP5-8.5 scenario to 5 cm in 2024. In the D-type climate, thickness varies from 10 cm for Chita under present-day conditions to 8 cm in the 2080 SSP5-8.5 scenario. The E-type climate in Resolute requires the highest

levels, currently up to 24 cm, and down to 9 cm by 2080 under SSP5-8.5. These trends reflect projected temperature rises, which reduce heating loads and thus lower insulation needs. Comparing SSP1-2.6 and SSP5-8.5, insulation thickness increases by up to 20 percent in C-type, 10 percent in D-type, and 13 percent in E-type climates.

Table 10. Summary of optimal retrofit measures derived from the decision-making phase in different time frames and climate zones.

Time Frame	Decision Variable	Cébazat	Chita	Resolute
2024	EW thickness (cm)	5	10	24
	W U-value ($W/m^2.K$)	0.58	0.54	0.45
	R thickness (cm)	5	9	13
	HS (°C)	21.1	22.5	22
	IR (ACH)	0.15	0.12	0.13
	Number of PV	155	208	233
	Number of SC	15	28	40
	Number of WT	1	4	7
2050 SSP1	EW thickness (cm)	5	9	17
	W U-value ($W/m^2.K$)	0.6	0.56	0.51
	R thickness (cm)	5	8	8
	HS (°C)	20.8	21.5	21.5
	IR (ACH)	0.14	0.15	0.15
	Number of PV	143	201	233
	Number of SC	13	22	33
	Number of WT	1	3	5
2080 SSP1	EW thickness (cm)	4	9	10
	W U-value ($W/m^2.K$)	0.62	0.57	0.53
	R thickness (cm)	7	7	7
	HS (°C)	20.4	21	21.5
	IR (ACH)	0.11	0.11	0.14
	Number of PV	133	198	210
	Number of SC	10	17	28
	Number of WT	1	3	3
2050 SSP5	EW thickness (cm)	3	8	10
	W U-value ($W/m^2.K$)	0.77	0.75	0.75
	R thickness (cm)	4	6	7
	HS (°C)	19.3	20.6	21.5
	IR (ACH)	0.14	0.16	0.15
	Number of PV	120	183	200
	Number of SC	10	16	23
	Number of WT	1	1	3
2080 SSP5	EW thickness (cm)	3	8	9
	W U-value ($W/m^2.K$)	0.87	0.85	0.8
	R thickness (cm)	2	3	6
	HS (°C)	19.2	19	21
	IR (ACH)	0.14	0.16	0.14
	Number of PV	115	165	190
	Number of SC	9	13	18
	Number of WT	1	1	2

EW thickness: External Wall insulation thickness, W U-value: Window U-value, R thickness: Roof insulation thickness, HS: Heating Setpoint, IR: Infiltration rate, Number of PV: Number of photovoltaics, Number of SC: Number of solar collectors, Number of WT: Number of Wind Turbines, ACH: Air change per hour, cm: centimeter, and °C: Celsius.

Window U-values also adjust with climate severity and time frame. In C-type climates, values range from 0.58 $W/m^2 \cdot K$ currently to 0.87 $W/m^2 \cdot K$ by 2080 SSP5-8.5. In D-type

climates, they vary from 0.54 W/m^2·K in the current period to 0.85 W/m^2·K under the 2080 SSP5-8.5 scenario. In the E-type climate, U-values rise from 0.45 W/m^2·K in the current period to 0.80 W/m^2·K by 2080 under SSP5-8.5. Higher U-values in warmer scenarios suggest that reduced window insulation can still maintain comfort as outdoor temperatures rise.

Infiltration rates remain relatively constant, with minor increases of approximately 25 percent in Resolute and Chita under SSP5-8.5. These changes suggest a trade-off between airtightness for energy efficiency and natural ventilation for indoor air quality.

Heating setpoints are maintained between 19.2 °C and 22.5 °C across all zones and time frames, exhibiting a slight downward trend as insulation improves and heating loads decline. Occupant comfort is preserved, since the optimization process minimizes PPD.

The number of photovoltaic panels and solar collectors decreases from 2024 through 2050 and 2080, especially under SSP5-8.5, with reductions of 34 percent in C-type climates, 42 percent in D-type climates, and 20 percent in E-type climates. These declines correspond to lower heating demands in warmer futures. The number of wind turbines remains constant in Cébazat but varies in D- and E-type zones. In Chita, the turbine count decreases from four currently to one by 2080 SSP5-8.5. In Resolute, turbines decrease from seven to two over the same interval. These results imply that wind energy potential is relatively stable in C-type climates but varies substantially in colder regions.

Table 11 reports the optimal annual energy consumption and PPD achieved for each climate zone and time frame following the decision-making phase. Energy savings range from 51% to 81% and PPD reductions from 54% to 67% across the examined scenarios, demonstrating substantial improvements in both energy efficiency and occupant comfort.

Table 11. Summary of optimal annual energy consumption and PPD savings.

Time Frame	Climate Zone	Energy Consumption		PPD	
		Optimal (kWh/[Year.m^2])	Saving (%)	Optimal (%)	Saving (%)
2024	Cébazat	38.36	58.70%	5.73	55.35%
	Chita	40.67	69.40%	6.889	61.14%
	Resolute	44.83	81.65%	8.043	67.07%
2050 SSP1	Cébazat	38.21	55.18%	5.39	55.28%
	Chita	39.06	66.90%	6.63	58.36%
	Resolute	38.49	76.20%	7.43	55.82%
2080 SSP1	Cébazat	37.90	54.50%	5.31	55.32%
	Chita	38.90	66.30%	6.60	58.43%
	Resolute	37.55	75.90%	7.47	54.84%
2050 SSP5	Cébazat	37.76	54.48%	5.268	54.97%
	Chita	37.76	65.50%	6.546	57.19%
	Resolute	37.76	75.36%	7.563	54.36%
2080 SSP5	Cébazat	37.75	51.50%	5.002	54.95%
	Chita	37.31	65.05%	6.522	55.42%
	Resolute	35.33	75.50%	7.295	54.07%

In climate type C, annual energy consumption decreases by 38.36% in 2024 and by 51.50% in 2080 under SSP5-8.5 relative to the base case. Projected PPD reductions in this zone range from 55.35% in 2024 to 54.95% in 2080 SSP5-8.5. For climate type D, energy consumption is reduced by 69.40% in 2024 and by 65.05% in 2080 under SSP5-8.5. Corresponding PPD savings lie between 61.14% and 55.42%. Climate type E (Resolute) achieves the highest energy savings, reaching 81.65% in 2024 and 75.30% in 2080

under SSP5-8.5. These large gains reflect the zone's higher baseline heating loads and the effectiveness of passive measures in extreme cold conditions.

When compared with findings in the literature, Ibrahim et al. [32] reviewed recent studies on retrofitting strategies for achieving nearly zero-energy buildings (NZEBs) and reported an average potential energy reduction of approximately 65.14%. They also found that the U-values of windows varied between 0.45 and 0.86 $W/m^2 \cdot K$ for climate types C, D, and E under current climatic conditions. However, that study did not examine the relative performance of retrofit measures under future climate scenarios, which represents a key contribution of the present work. In addition, Ibrahim et al. [78] reported average airtightness values of 0.15, 0.16, and 0.13 ACH for climate types C, D, and E, respectively, results that are in close agreement with the ranges observed in this study.

The stronger absolute energy-saving effect in colder zones can be explained primarily by higher baseline heating demand and by nonlinear marginal gains from insulation improvements. Where baseline heating consumption is large, envelope upgrades and airtightness measures produce larger absolute reductions because they target the dominant end-use directly. Marginal savings are greatest when initial thermal resistance is low; once a high insulation level is reached, incremental gains diminish. Additionally, the interaction with renewable generation and the temporal match between generation and residual load modifies net savings across zones: identical envelope upgrades yield different net energy benefits depending on local resource availability and load shape. Projected warming reduces heating-degree-days in future horizons, which lowers absolute savings potential and partly explains the smaller gains observed under SSP5-8.5 relative to the present day.

The results indicate clear potential for informing NZEB retrofit policy and adaptation strategies. Building-level sustainability assessment, including both embodied and operational impacts, is essential to ensure environmentally sound interventions. Reductions in renewable system requirements under warmer futures may lower capital costs but interact with policy instruments such as subsidies, feed-in tariffs, or grid integration requirements. Life-cycle cost analysis and payback assessments would further enhance the practical relevance of the results. Consideration of supply chain constraints and phased retrofit strategies can facilitate realistic implementation in the built environment.

Several uncertainties may influence the robustness of these results. Climatic uncertainty arises from the limited SSP selection and the variability of climate model projections; future work should incorporate CMIP6 ensemble projections. Surrogate uncertainty associated with the ANN also requires evaluation through cross-validation, hold-out testing, or ensemble approaches to quantify prediction error. Finally, only a single prototypical building with simplified façade and HVAC representation was analyzed; hence, generalization to other building archetypes is limited. The results should be interpreted as exploratory, illustrating methodological potential rather than serving as universal prescriptions.

The practical application of this work lies in providing a rapid, scenario-aware tool for NZEB retrofit planning, supporting policy design and investment decision-making. The primary scientific contribution is the integration of ANN-based surrogates with NSGA-III multi-objective optimization and TOPSIS ranking under multiple climate scenarios, which enables efficient mapping of energy-comfort trade-offs. Future research should focus on empirical validation, extension to diverse building types and HVAC systems, incorporation of climate model ensembles to account for uncertainty, and integration of life-cycle economic and environmental metrics such as LCC and embodied carbon into the optimization framework.

4. Conclusions

This study demonstrates that an ANN-based surrogate, integrated with NSGA-III multi-objective optimization and TOPSIS ranking, provides an effective and computationally efficient framework for designing NZEB retrofit strategies under multiple future climate scenarios. Quantitative results indicate that integrated passive and renewable retrofits can reduce annual energy consumption by 45–81% and decrease PPD by 54–67% across the examined scenarios and climate zones, with maximum improvements of approximately 81% in energy consumption and 67% in PPD. These gains are achieved while maintaining net-zero energy balance constraints and exploring trade-offs between energy use and thermal comfort.

The study makes several key contributions. First, it demonstrates the development and application of an ANN surrogate to accelerate building energy simulations and enable exhaustive multi-objective optimization across multiple climate futures. Second, it illustrates the coupling of NSGA-III with TOPSIS to map Pareto trade-offs and provide a transparent ranking of preferred retrofit packages. Third, it shows how optimal retrofit portfolios shift under contrasting SSP scenarios (SSP1-2.6 vs. SSP5-8.5) and across seven heating-dominant Köppen–Geiger zones. Rising temperatures are found to reduce heating demand and modify optimal insulation and glazing specifications, with relative decreases in required insulation thickness and increases in optimal window U-values under warmer, fossil-intensive futures, while PV and solar collector sizing reflect changing seasonal loads.

The findings have practical implications. For policymakers and building practitioners, the results highlight the importance of incorporating future climate projections into retrofit planning and building codes, ensuring that insulation and renewable energy systems are neither over- nor undersized. For industry, surrogate-assisted optimization offers a scalable tool for rapid, scenario-aware assessment of retrofit options, supporting product specification, supply chain planning, and phased investment strategies.

This work also has limitations that motivate further research. It focused on a single prototypical building with limited façade and HVAC detail and considered only two SSPs, which restricts generalizability across building types, HVAC systems, and climate model ensembles. Future studies should apply the workflow to diverse building stocks, incorporate CMIP6 ensemble projections to account for climate-model uncertainty, extend the ANN/morphing framework to region-specific design and HVAC configurations, and integrate economic and life-cycle metrics, such as LCC and embodied emissions, for cost-optimal, low-carbon decision-making. Additionally, exploring transfer learning and robustness/uncertainty-aware optimization could improve surrogate generalization and practical applicability. Implementing these extensions will enhance methodological rigor and increase the operational utility of ANN-assisted multi-objective retrofit optimization under climate change.

Author Contributions: Conceptualization, M.I.; Methodology, M.I.; Software, M.I.; Validation, M.I.; Formal analysis, M.I.; Writing—original draft, M.I.; Supervision, P.B. and F.H.; Visualization F.F. and S.E.O. All authors have read and agreed to the published version of the manuscript.

Funding: This research was funded by Le Department de l'Allier" and University of Clermont Auvergne ISITE CAP 20-25 program. And The APC was funded by Ms. Eveline Cheng.

Data Availability Statement: The original contributions presented in this study are included in the article. Further inquiries can be directed to the corresponding author.

Conflicts of Interest: The authors declare no conflict of interest.

Abbreviations

The following abbreviations are used in this manuscript:

NZEB	Net-zero energy building
BES	Building energy simulation
TMY	Typical Meteorological Year
NSGA-III	Non-Dominated Sorting Genetic Algorithm
TOPSIS	Technique for Order of Preference by Similarity to Ideal Solution
MOO	Multi-Objective Optimization
ANN	Artificial Neural Networks
SVM	Support Vector Machines
MCDM	Multi-Criteria Decision-Making
G-value	Solar Heat Gain Coefficient
DHW	Domestic Hot Water
AHP	Analytic Hierarchy Process
PMV	Predicted Mean Vote
SDHW	Solar Domestic Hot Water
TRNSYS	Transient System Simulation Tool
MOHO-ANN	Multi-Objective Hyperparameter Optimization of ANN
GELU	Gaussian Error Linear Unit
R^2	Coefficient of Determination
SSP	Shared Socioeconomic Pathways

References

1. United Nations. Population. Available online: https://www.un.org/en/global-issues/population (accessed on 21 March 2023).
2. IEA. Buildings–Topics. Available online: https://www.iea.org/topics/buildings (accessed on 26 September 2022).
3. IEA—International Energy Agency. Available online: https://www.iea.org (accessed on 23 April 2024).
4. Harkouss, F.; Fardoun, F.; Biwole, P.H. Multi-objective optimization methodology for net zero energy buildings. *J. Build. Eng.* **2018**, *16*, 57–71. [CrossRef]
5. Harkouss, F.; Fardoun, F.; Biwole, P.H. Optimization approaches and climates investigations in NZEB—A review. *Build. Simul.* **2018**, *11*, 923–952. [CrossRef]
6. Alaifan, B.; Azar, E. Potential for Net-Zero Energy Communities in Kuwait: An Empirical Techno-Economic Modeling and Optimization Approach. *Buildings* **2023**, *13*, 2096. [CrossRef]
7. Júnior, S.M.; Frandoloso, M.A.L.; Brião, V.B. Technical and economic feasibility study for a university zero energy building in Southern Brazil. *Energy Build.* **2023**, *281*, 112748. [CrossRef]
8. Chacón, L.; Austin, M.C.; Castaño, C. A Multiobjective Optimization Approach for Retrofitting Decision-Making towards Achieving Net-Zero Energy Districts: A Numerical Case Study in a Tropical Climate. *Smart Cities* **2022**, *5*, 405–432. [CrossRef]
9. Luo, X.J. Retrofitting existing office buildings towards life-cycle net-zero energy and carbon. *Sustain. Cities Soc.* **2022**, *83*, 103956. [CrossRef]
10. Mata, É.; Wanemark, J.; Nik, V.M.; Kalagasidis, A.S. Economic feasibility of building retrofitting mitigation potentials: Climate change uncertainties for Swedish cities. *Appl. Energy* **2019**, *242*, 1022–1035. [CrossRef]
11. Thomas, A.; Menassa, C.C.; Kamat, V.R. A systems simulation framework to realize net-zero building energy retrofits. *Sustain. Cities Soc.* **2018**, *41*, 405–420. [CrossRef]
12. Cui, Y.; Yan, D.; Hong, T.; Xiao, C.; Luo, X.; Zhang, Q. Comparison of typical year and multiyear building simulations using a 55-year actual weather data set from China. *Appl. Energy* **2017**, *195*, 890–904. [CrossRef]
13. Chai, J.; Huang, P.; Sun, Y. Differential evolution-based system design optimization for net zero energy buildings under climate change. *Sustain. Cities Soc.* **2020**, *55*, 102037. [CrossRef]
14. Li, H.; Yang, Y.; Lv, K.; Liu, J.; Yang, L. Compare several methods of select typical meteorological year for building energy simulation in China. *Energy* **2020**, *209*, 118465. [CrossRef]
15. Guo, J.; Xia, D.; Zhang, L.; Zou, Y.; Yang, X.; Xie, W.; Zhong, Z. Future indoor overheating risk for urban village housing in subtropical region of China under long-term changing climate. *Build. Environ.* **2023**, *246*, 110978. [CrossRef]
16. Neto, A.H.; Durante, L.C.; Callejas, I.J.A.; da Guarda, E.L.A.; Moreira, J.V.R. The challenges on operating a zero net energy building facing global warming conditions. *Build. Simul.* **2022**, *15*, 435–451. [CrossRef]

17. Luo, X.J.; Oyedele, L.O. Life cycle optimisation of building retrofitting considering climate change effects. *Energy Build.* **2022**, *258*, 111830. [CrossRef]
18. Shen, P.; Lior, N. Vulnerability to climate change impacts of present renewable energy systems designed for achieving net-zero energy buildings. *Energy* **2016**, *114*, 1288–1305. [CrossRef]
19. Shen, P.; Braham, W.; Yi, Y. The feasibility and importance of considering climate change impacts in building retrofit analysis. *Appl. Energy* **2019**, *233–234*, 254–270. [CrossRef]
20. Kim, H.; Clayton, M.J. A multi-objective optimization approach for climate-adaptive building envelope design using parametric behavior maps. *Build. Environ.* **2020**, *185*, 107292. [CrossRef]
21. Li, Z.; Zhao, Y.; Xia, H.; Xie, S. A multi-objective optimization framework for building performance under climate change. *J. Build. Eng.* **2023**, *80*, 107978. [CrossRef]
22. Zou, Y.; Lou, S.; Xia, D.; Lun, I.Y.F.; Yin, J. Multi-objective building design optimization considering the effects of long-term climate change. *J. Build. Eng.* **2021**, *44*, 102904. [CrossRef]
23. Westermann, P.; Evins, R. Surrogate modelling for sustainable building design—A review. *Energy Build.* **2019**, *198*, 170–186. [CrossRef]
24. Starke, A.R.; Da Silva, A.K. A review on the applicability of machine learning techniques to the metamodeling of energy systems. *Numer. Heat Transf. Part B Fundam.* **2025**, *86*, 214–243. [CrossRef]
25. Zhan, J.; He, W.; Huang, J. Dual-objective building retrofit optimization under competing priorities using Artificial Neural Network. *J. Build. Eng.* **2023**, *70*, 106376. [CrossRef]
26. Aruta, G.; Ascione, F.; Bianco, N.; Iovane, T.; Mauro, G.M. ANN-based model predictive control for optimizing space cooling management. *Energy* **2025**, *328*, 136469. [CrossRef]
27. Zhang, H.; Feng, H.; Hewage, K.; Arashpour, M. Artificial Neural Network for Predicting Building Energy Performance: A Surrogate Energy Retrofits Decision Support Framework. *Buildings* **2022**, *12*, 829. [CrossRef]
28. Knauf XTherm ITEx Sun+. Panneau Isolant Extérieur–Isolation PSE Sous Enduits Minces ou Epais–Knauf. Available online: https://www.knauf.fr/solutions/produit/knauf-xtherm-itex-sun-plus (accessed on 14 November 2023).
29. *ISO 18523-2:2018*; Energy Performance of Buildings—Schedule and Condition of Building, Zone and Space Usage for Energy Calculation—Part 2: Residential Buildings. ISO: Geneva, Switzerland, 2018.
30. *NF EN 625*; Gas Fired Central Heating Boilers. Specific Requirements for the Domestic Hot Water Operation of Combination Boilers of Nominal Heat Input Not Exceeding 70 kw. AFNOR: La Plaine Saint-Denis, France, 1995.
31. Home Page–ADEME, The French Agency for Ecological Transition. Available online: https://www.ademe.fr/en/frontpage/ (accessed on 8 April 2024).
32. Ibrahim, M.; Harkouss, F.; Biwole, P.; Fardoun, F.; Ouldboukhitine, S. Building retrofitting towards net zero energy: A review. *Energy Build.* **2024**, *322*, 114707. [CrossRef]
33. Roman, N.D.; Bre, F.; Fachinotti, V.D.; Lamberts, R. Application and characterization of metamodels based on artificial neural networks for building performance simulation: A systematic review. *Energy Build.* **2020**, *217*, 109972. [CrossRef]
34. Harkouss, F.; Fardoun, F.; Biwole, P.H. Passive design optimization of low energy buildings in different climates. *Energy* **2018**, *165*, 591–613. [CrossRef]
35. Tian, Z.; Zhang, X.; Wei, S.; Du, S.; Shi, X. A review of data-driven building performance analysis and design on big on-site building performance data. *J. Build. Eng.* **2021**, *41*, 102706. [CrossRef]
36. Kočí, J.; Kočí, V.; Maděra, J.; Černý, R. Effect of applied weather data sets in simulation of building energy demands: Comparison of design years with recent weather data. *Renew. Sustain. Energy Rev.* **2019**, *100*, 22–32. [CrossRef]
37. Liu, Y.; Stouffs, R.; Tablada, A.; Wong, N.H.; Zhang, J. Comparing micro-scale weather data to building energy consumption in Singapore. *Energy Build.* **2017**, *152*, 776–791. [CrossRef]
38. Bracht, M.K.; Melo, A.P.; Lamberts, R. A metamodel for building information modeling-building energy modeling integration in early design stage. *Autom. Constr.* **2021**, *121*, 103422. [CrossRef]
39. Thrampoulidis, E.; Mavromatidis, G.; Lucchi, A.; Orehounig, K. A machine learning-based surrogate model to approximate optimal building retrofit solutions. *Appl. Energy* **2021**, *281*, 116024. [CrossRef]
40. Ibrahim, M.; Harkouss, F.; Biwole, P.; Fardoun, F.; Oultboukhtine, S. Building retrofitting towards net zero energy under climate change. *J. Phys. Conf. Ser.* **2024**, *2857*, 012026. [CrossRef]
41. Regulus. Solar Collectors. Available online: https://www.regulus.eu/en/solar-collectors (accessed on 27 March 2024).
42. Bataineh, K.; Dalalah, D. Optimal Configuration for Design of Stand-Alone PV System. *Smart Grid Renew. Energy* **2012**, *3*, 139–147. [CrossRef]
43. Kamali, S. Feasibility analysis of standalone photovoltaic electrification system in a residential building in Cyprus. *Renew. Sustain. Energy Rev.* **2016**, *65*, 1279–1284. [CrossRef]
44. *SUNNY TRIPOWER 5000TL-12000TL—The Three-Phase Inverter—Not Only for Your Home…*; SMA Solar Technology: Niestetal, Germany, 2017; Volume 150.

45. Nafeh, A.E.-S.A. Design and Economic Analysis of a Stand-Alone PV System to Electrify a Remote Area Household in Egypt. *Open Renew. Energy J.* **2009**, *2*, 33–37. [CrossRef]
46. Norton, P.; Christensen, C.; Hancock, E.; Barker, G.; Reeves, P. *NREL/Habitat for Humanity Zero Energy Home: A Cold-Climate Case Study for Affordable Zero Energy Homes*; NREL/TP-550-43188; National Renewable Energy Lab. (NREL): Golden, CO, USA, 2008. [CrossRef]
47. Home-Mitsubishi Electric. Available online: https://www.mitsubishi-pv.de/index-service_en.php (accessed on 27 March 2024).
48. Raum Energy 3.5—3,50 kW—Wind Turbine. Available online: https://en.wind-turbine-models.com/turbines/1071-raum-energy-3.5 (accessed on 27 March 2024).
49. Dutta, S.; Gandomi, A.H. Design of experiments for uncertainty quantification based on polynomial chaos expansion metamodels. In *Handbook of Probabilistic Models*; Elsevier: Amsterdam, The Netherlands, 2020; pp. 369–381. [CrossRef]
50. Jones, D.R.; Schonlau, M.; Welch, W.J. Efficient Global Optimization of Expensive Black-Box Functions. *J. Glob. Optim.* **1998**, *13*, 455–492. [CrossRef]
51. Abbass, M.A.B. A comprehensive framework based on Bayesian optimization and skip connections artificial neural networks to predict buildings energy performance. *J. Build. Eng.* **2023**, *77*, 107523. [CrossRef]
52. Paszke, A.; Gross, S.; Massa, F.; Lerer, A.; Bradbury, J.; Chanan, G.; Killeen, T.; Lin, Z.; Gimelshein, N.; Antiga, L.; et al. PyTorch: An Imperative Style, High-Performance Deep Learning Library. *arXiv* **2019**, arXiv:1912.01703. [CrossRef]
53. Blank, J.; Deb, K. Pymoo: Multi-Objective Optimization in Python. *IEEE Access* **2020**, *8*, 89497–89509. [CrossRef]
54. El Kounni, A.; Outzourhit, A.; Mastouri, H.; Radoine, H. Building energy model automated calibration using Pymoo. *Energy Build.* **2023**, *298*, 113524. [CrossRef]
55. *ANSI/ASHRAE Standard 228*; Standard Method of Evaluating Zero Net Energy and Zero Net Carbon Building Performance. ASHRAE: Peachtree Corners, GA, USA, 2023.
56. Ibrahim, M.; Harkouss, F.; Biwole, P.; Ouldboukhitine, S.; Fardoun, F. Calibration of a Building Energy Simulation Using a Multi-step Method. In Proceedings of the Sixth International Conference on Efficient Building Design, Beirut, Lebanon, 7–8 November 2024; ASHRAE: Peachtree Corners, GA, USA, 2025. [CrossRef]
57. Ibrahim, M.; Harkouss, F.; Biwole, P.; Fardoun, F.; Ouldboukhitine, S.-E. Multi-objective hyperparameter optimization of artificial neural network in emulating building energy simulation. *Energy Build.* **2025**, *337*, 115643. [CrossRef]
58. Seada, H.; Deb, K. A Unified Evolutionary Optimization Procedure for Single, Multiple, and Many Objectives. *IEEE Trans. Evol. Comput.* **2016**, *20*, 358–369. [CrossRef]
59. Sartori, I.; Napolitano, A.; Voss, K. Net zero energy buildings: A consistent definition framework. *Energy Build.* **2012**, *48*, 220–232. [CrossRef]
60. Lai, Y.-J.; Liu, T.-Y.; Hwang, C.-L. TOPSIS for MODM. *Eur. J. Oper. Res.* **1994**, *76*, 486–500. [CrossRef]
61. Kilkis, B. Net-zero buildings, what are they and what they should be? *Energy* **2022**, *256*, 124442. [CrossRef]
62. Deng, H.; Yeh, C.-H.; Willis, R.J. Inter-company comparison using modified TOPSIS with objective weights. *Comput. Oper. Res.* **2000**, *27*, 963–973. [CrossRef]
63. Wang, E.; Alp, N.; Shi, J.; Wang, C.; Zhang, X.; Chen, H. Multi-criteria building energy performance benchmarking through variable clustering based compromise TOPSIS with objective entropy weighting. *Energy* **2017**, *125*, 197–210. [CrossRef]
64. Deb, K.; Jain, H. An Evolutionary Many-Objective Optimization Algorithm Using Reference-Point-Based Nondominated Sorting Approach, Part I: Solving Problems with Box Constraints. *IEEE Trans. Evol. Comput.* **2014**, *18*, 577–601. [CrossRef]
65. Si, J.; Marjanovic-Halburd, L.; Nasiri, F.; Bell, S. Assessment of building-integrated green technologies: A review and case study on applications of Multi-Criteria Decision Making (MCDM) method. *Sustain. Cities Soc.* **2016**, *27*, 106–115. [CrossRef]
66. Delgarm, N.; Sajadi, B.; Delgarm, S.; Kowsary, F. A novel approach for the simulation-based optimization of the buildings energy consumption using NSGA-II: Case study in Iran. *Energy Build.* **2016**, *127*, 552–560. [CrossRef]
67. Andreolli, F.; Bragolusi, P.; D'Alpaos, C.; Faleschini, F.; Zanini, M.A. An AHP model for multiple-criteria prioritization of seismic retrofit solutions in gravity-designed industrial buildings. *J. Build. Eng.* **2022**, *45*, 103493. [CrossRef]
68. Liu, Y.; Chen, H.; Wang, X. Research on green renovations of existing public buildings based on a cloud model–TOPSIS method. *J. Build. Eng.* **2021**, *34*, 101930. [CrossRef]
69. Marzouk, M.; El-Maraghy, M.; Metawie, M. Assessing retrofit strategies for mosque buildings using TOPSIS. *Energy Rep.* **2023**, *9*, 1397–1414. [CrossRef]
70. Stanojević, A.D.; Milošević, M.R.; Milošević, D.M.; Turnšek, B.A.; Jevremović, L.L. Developing multi-criteria model for the protection of built heritage from the aspect of energy retrofitting. *Energy Build.* **2021**, *250*, 111285. [CrossRef]
71. Saaty, T.L. A scaling method for priorities in hierarchical structures. *J. Math. Psychol.* **1977**, *15*, 234–281. [CrossRef]
72. Saaty, T.L. Decision making—The Analytic Hierarchy and Network Processes (AHP/ANP). *J. Syst. Sci. Syst. Eng.* **2004**, *13*, 1–35. [CrossRef]

73. Hausfather, Z. Explainer: How 'Shared Socioeconomic Pathways' Explore Future Climate Change. Available online: https://www.carbonbrief.org/explainer-how-shared-socioeconomic-pathways-explore-future-climate-change/ (accessed on 7 May 2024).
74. Riahi, K.; Van Vuuren, D.P.; Kriegler, E.; Edmonds, J.; O'Neill, B.C.; Fujimori, S.; Bauer, N.; Calvin, K.; Dellink, R.; Fricko, O.; et al. The Shared Socioeconomic Pathways and their energy, land use, and greenhouse gas emissions implications: An overview. *Glob. Environ. Change* **2017**, *42*, 153–168. [CrossRef]
75. SSP Database. Available online: https://tntcat.iiasa.ac.at/SspDb/dsd?Action=htmlpage&page=welcome (accessed on 7 May 2024).
76. Mostafaei, H.; Barmchi, M.A.; Bahmani, H. Seismic Resilience and Sustainability: A Comparative Analysis of Steel and Reinforced Structures. *Buildings* **2025**, *15*, 1613. [CrossRef]
77. Kottek, M.; Grieser, J.; Beck, C.; Rudolf, B.; Rubel, F. World Map of the Köppen-Geiger climate classification updated. *Meteorol. Z.* **2006**, *15*, 259–263. [CrossRef]
78. Ibrahim, M.; Biwole, P.; Ouldboukhitine, S.E.; Harkouss, F.; Fardoun, F. Hyperparameter optimization of artificial neural network in building energy simulation. In Proceedings of the Conférence IBPSA France 2024 & Ecole Thématique SIMUREX, La Rochelle, France, 13–17 May 2024.

Disclaimer/Publisher's Note: The statements, opinions and data contained in all publications are solely those of the individual author(s) and contributor(s) and not of MDPI and/or the editor(s). MDPI and/or the editor(s) disclaim responsibility for any injury to people or property resulting from any ideas, methods, instructions or products referred to in the content.